

RESEARCH ARTICLE

10.1002/2015JB012604

Key Points:

- Upper mantle anisotropy under the Carpathian-Pannonian Region is constrained by shear wave splitting
- Results show a remarkable large-scale simple anisotropy pattern under the whole region
- A possible model to explain the NW-SE anisotropy within the asthenospheric mantle is presented

Supporting Information:

- Supporting Information S1
- Table S1

Correspondence to:

E. Qorbani,
ehsan.qorbani@univie.ac.at

Citation:

Qorbani, E., G. Bokelmann, I. Kovács, F. Horváth, and G. Falus (2016), Deformation in the asthenospheric mantle beneath the Carpathian-Pannonian Region, *J. Geophys. Res. Solid Earth*, 121, doi:10.1002/2015JB012604.

Received 16 OCT 2015

Accepted 28 AUG 2016

Accepted article online 3 SEP 2016

Deformation in the asthenospheric mantle beneath the Carpathian-Pannonian Region

Ehsan Qorbani¹, Götz Bokelmann¹, István Kovács², Frank Horváth³, and György Falus²

¹Department of Meteorology and Geophysics, University of Vienna, Vienna, Austria, ²Geological and Geophysical Institute of Hungary, Budapest, Hungary, ³Geomega Ltd., Budapest, Hungary

Abstract To better understand the evolution and present-day tectonics of the Carpathian-Pannonian Region (CPR), we characterize the upper mantle anisotropic structure. We present a shear wave splitting analysis from teleseismic events recorded at the Carpathian Basin Project and permanent stations located in the CPR. The results show a large-scale uniform NW-SE fast orientation under the entire CPR. Compared with the complexity of geologic structures, the anisotropy expresses a relatively simple pattern of deformation. We attribute this anisotropy to an asthenospheric origin and interpret it as flow-induced alignments within the upper mantle. We also observe a few measurements depicting NE-SW fast orientation in line with the Mid-Hungarian Shear Zone. This suggests the likely contribution of either lithosphere or northeastward flow into a slab gap under the northern Dinarides. We observe splitting delay times on average of 1 s, showing noticeable change (60%) in the middle Pannonian basin. This change correlates well with the variation in the thickness of low-velocity zones that were previously imaged between a depth of 75 and 400 km by velocity tomography. In order to evaluate the relation between anisotropy and tectonics, we compare our data with the tectonic models that have so far been suggested to explain the evolution and current-stage tectonics of the region. We present here a plausible tectonic model responsible for the NW-SE anisotropy within the asthenospheric mantle. In this model, NW-SE deformation is mainly generated in a northeastward compressional tectonic regime acting in a wide region between the Adriatic microplate and the East European platform.

1. Introduction

Seismic anisotropy is manifested by a directional dependence of seismic velocity. Within the upper mantle, it is generated mostly by development of the crystallographic orientation of (olivine and pyroxene) minerals in response to deformation [Nicolas *et al.*, 1973; Long and Becker, 2010]. Observing seismic anisotropy can therefore be used to describe the strain distribution in the upper mantle, in turn, reflecting the deformation patterns, active flow geometry, and also the conditions in which the rock is deformed [e.g., Karato *et al.*, 2008; Vauchez *et al.*, 2012]. These observations allow us to address what happens at a depth where stress and strain cannot be measured directly.

The Carpathian-Pannonian Region (CPR) is located at the northeastern end of the Alpine mountain belt in Europe (Figure 1). It consists of a variety of geological structures and tectonic units resulting from subduction, plate collision, basin evolution, and thrust faulting. A large part of the CPR is occupied by the Pannonian basin, which is surrounded by the Alps, Dinarides, and Carpathians (Figure 1). In order to get insight into the origin of the extensional basins within the CPR, the Carpathian Basin Project (CBP) was established [Houseman and Stuart, 2011]. Alongside several seismological studies such as (body wave) velocity tomography [e.g., Dando *et al.*, 2011; Ren *et al.*, 2012] and *P* wave receiver functions analysis [Hetényi *et al.*, 2015] which have been done using the CBP data, the upper mantle anisotropy has previously been studied through *SKS* splitting [Houseman and Stuart, 2011]. While some of the results of that study agree with other recently published anisotropy data of the Eastern Alps and south Bohemia, some do not. For instance, Houseman and Stuart [2011] presented E-W fast orientation for the stations located in the middle and northwest of the CBP profiles, while the permanent stations in that area [Bokelmann *et al.*, 2013; Qorbani *et al.*, 2015], and in the nearby area [Plomerova *et al.*, 2012], showed NW-SE anisotropy.

Here we reprocess *SKS* and *SKKS* splitting parameters (fast polarization azimuth and delay time) from data recorded by the CBP and a number of permanent stations of the Hungarian Seismic Network. We also consider

01
02
03
04
05
06
07
08
09
10
11
12
13
14
15
16
17
18
19
20
21
22
23
24
25
26
27
28
29
30
31
32
33
34
35
36
37
38
39
40
41
42
43
44
45
46
47
48
49
50
51
52
53
54
55

Q2

Q3

F1

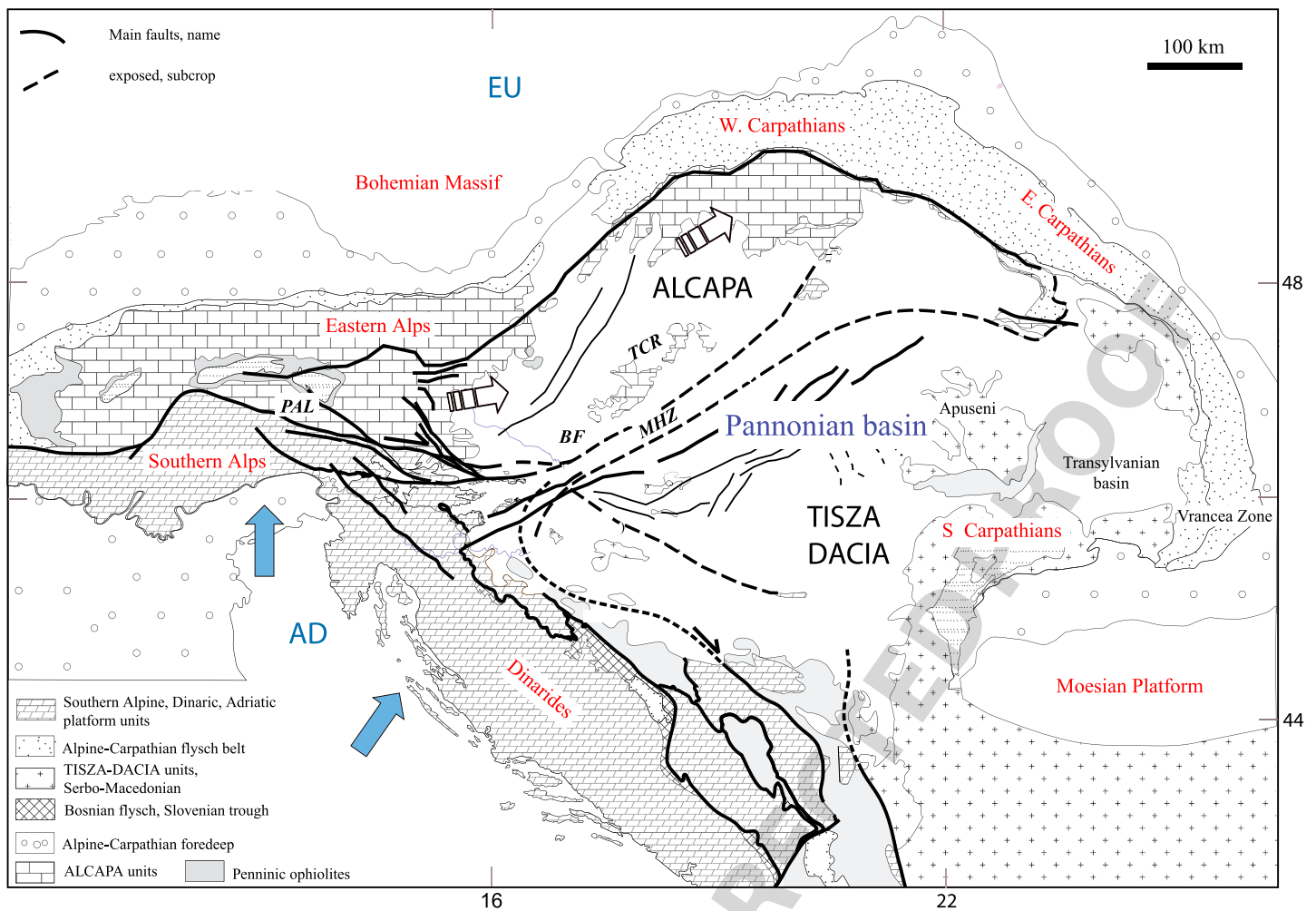


Figure 1. Spatial distribution of basement rocks and major tectonic units of the Carpathian-Pannonian Region. The Adriatic microplate has been indenting and pushing the Alpine-Dinaric belt since the Cretaceous, as indicated by blue arrow [Horváth *et al.*, 2006]. White arrow represents the lateral escape of the Alcapa unit. The map has been compiled and modified after Fodor *et al.* [1999] and Haas *et al.* [2000, and references therein]. BF: Balaton fault, TCR: Transdanubian Central Range, PAL: Periadriatic line, and MHZ: Mid-Hungarian Shear Zone. EU: European plate and AD: Adriatic microplate.

the models that have so far been suggested for the evolution and current-stage tectonics of the region, in terms of tectonic field responsible for induced anisotropy observed from the SKS splitting.

2. Tectonic Background

The CPR was formed in several major steps during the Late Cretaceous-Cenozoic [Schmid *et al.*, 2008]. The “hard collision” between the Adria and the stable European platform in the Eocene resulted in the subsequent onset of major lateral displacements along the main tectonic lines (e.g., Periadriatic line, Figure 1) and the consequent lateral escape of a tectonic block (Alcapa) toward the east [Ratschbacher *et al.*, 1991a; Fodor *et al.*, 1999]. The Pannonian basin comprises two major units, Alcapa and Tisza-Dacia (Figure 1), which have experienced different and complex extension processes [Horváth *et al.*, 2006; Schmid *et al.*, 2008]. The region that separates these two distinct units is the Mid-Hungarian Shear Zone (MHZ) where the Balaton fault is located on its northern margin (Figure 1). Clockwise rotation of the Tisza-Dacia block and counterclockwise rotation of the Alcapa block have been proposed; they took place mainly in the early Miocene [Márton *et al.*, 2000]. This was followed by the significant extension and formation of the Pannonian basin during the rest of the Miocene [Horváth, 1993, 2006, 2015]. The extension affected the lithospheric mantle more substantially than the crust where the lithosphere was thinned 4 to 8 times its original thickness [Huismans *et al.*, 2001]. The extension was followed by an episode of tectonic inversion in the past 5–10 Ma, which was the consequence of the docking of major tectonic units in the Carpathian embayment [Bada *et al.*, 2007].

There are controversial models for the most important driving force of lithospheric extension and formation of the Pannonian basin. For example, mantle plume(s) [Wilson and Downes, 1992] and diapir(s) [Stegena et al., 1975] were invoked as main driving mechanisms; the slab-rollback model [Horváth, 1993] attributing the extension of lithosphere to suction of the oceanic slab rolling back along the Carpathians; dripping of over thickened lithosphere along the Carpathians [Houseman and Gemmer, 2007]; asthenospheric flow as a result of trapping material between colliding continental lithospheres, the Adria and Europe [Kovács et al., 2012]; and rollback of the oceanic plate beneath the Apennines and the consequent inward flow entering the CPR [Horváth and Faccenna, 2011]. The latter models, however, all imply the potential and significant role of asthenospheric flow in the formation of the Pannonian basin. While the common point of these models is the asthenospheric flow, the authors share contrasting ideas about what is responsible for the generation of this flow. Our seismic anisotropy data may potentially have an important contribution to the ongoing controversy about the formation of the CPR.

3. Method and Data

We used the shear wave splitting method [e.g., Vinnik et al., 1984; Silver and Chan, 1988] to constrain anisotropy. This method has become a routine means of characterizing mantle anisotropy by analyzing the splitting of core shear waves, $SK(K)S$, during their voyage through anisotropic structures [Savage, 1999; Fouch and Rondenay, 2006]. Although lower mantle anisotropic minerals likely affect $SKKS$ splitting, due to our limited knowledge of the lower mantle deformation we assume that the major source of anisotropy is the upper mantle [Silver, 1996].

Splitting parameters, fast axis azimuth (ϕ), and splitting delay time (δt) between the fast and slow phases can be measured by several approaches. Here we simultaneously applied the following techniques; the waveform cross correlation [Bowman and Ando, 1987], linearizing the particle motion (minimizing the second eigenvalue of covariance matrix [Silver and Chan, 1991]), and transverse component minimization [Silver and Chan, 1991], by utilizing the SplitLab package [Wüstefeld et al., 2008]. Applying all of these techniques allows us to qualify the measurements as "good," "fair," and "poor" quality. The qualification criteria [following Barruol et al., 1997; Wüstefeld and Bokelmann, 2007] includes the agreement between results of different techniques (i.e., good quality is chosen if the difference in fast azimuth from three techniques is less than 10°), signal-to-noise ratios ($SNR > 5$), the ellipticity and linearity of particle motion before and after correction, and the confident region of the best fitting splitting parameters. After qualification, the results of the transverse component minimization approach (SC) were selected to characterize the upper mantle anisotropy.

We used data from 59 seismic stations (Figure 3). Among those, 53 temporary stations, as part of the Carpathian Basin Project (CBP), were already deployed on three parallel NW-SE oriented profiles with the station spacing of about 30 km (Figure 3). The stations consisted of 46 Guralp CMG-3TD (30 s period) sensors, and 10 Guralp CMG-3TD (120 s period) sensors. Recordings from these stations between 2005 and 2007 were used for our analysis. In order to improve the station coverage, data from six permanent stations of the Hungarian Seismological Network (HU) between 2004 and 2014 were also included in the data collection. The database includes teleseismic events occurring in an epicentral distance range from 90° to 130° with magnitudes greater than 5.75 (M_w). Most of the waveforms were band-pass-filtered between 0.01 Hz and 1 Hz and visually inspected to ensure the proper phase window selection and detection of clearly split $SK(K)S$ phases. Altogether 5689 $SK(K)S$ phases were visually examined in which 375 split shear waves were measured. Among them, 230 measures were selected as good quality. In addition, in the absence of significant energy on the transverse component, 109 splitting measurements were selected as good "null" from a total of 157 null measurements (Figure 2).

Examination of anisotropy in naturally deformed rock samples provides valuable information about the tectonic processes and mechanisms which develop deformation within the Earth's interior [Zhang and Karato, 1995]. In this study we used the petrofabric experimental results of natural rock samples. Samples are basalt-hosted upper mantle xenoliths taken from the Nógrád-Gömör Volcanic Field, NGVF [Klébesz et al., 2015], and from the Bakony-Balaton Highland (BBH) and Little Hungarian Plain (LHP) areas [Kovács et al., 2012, Figure 2]. According to prior geochemical and petrological analysis on the BBH and LHP samples, two main groups could be distinguished. The first group might represent the new juvenile part of the lithosphere which has been accreted from the asthenosphere since the end of the extension in the thermal relaxation stage

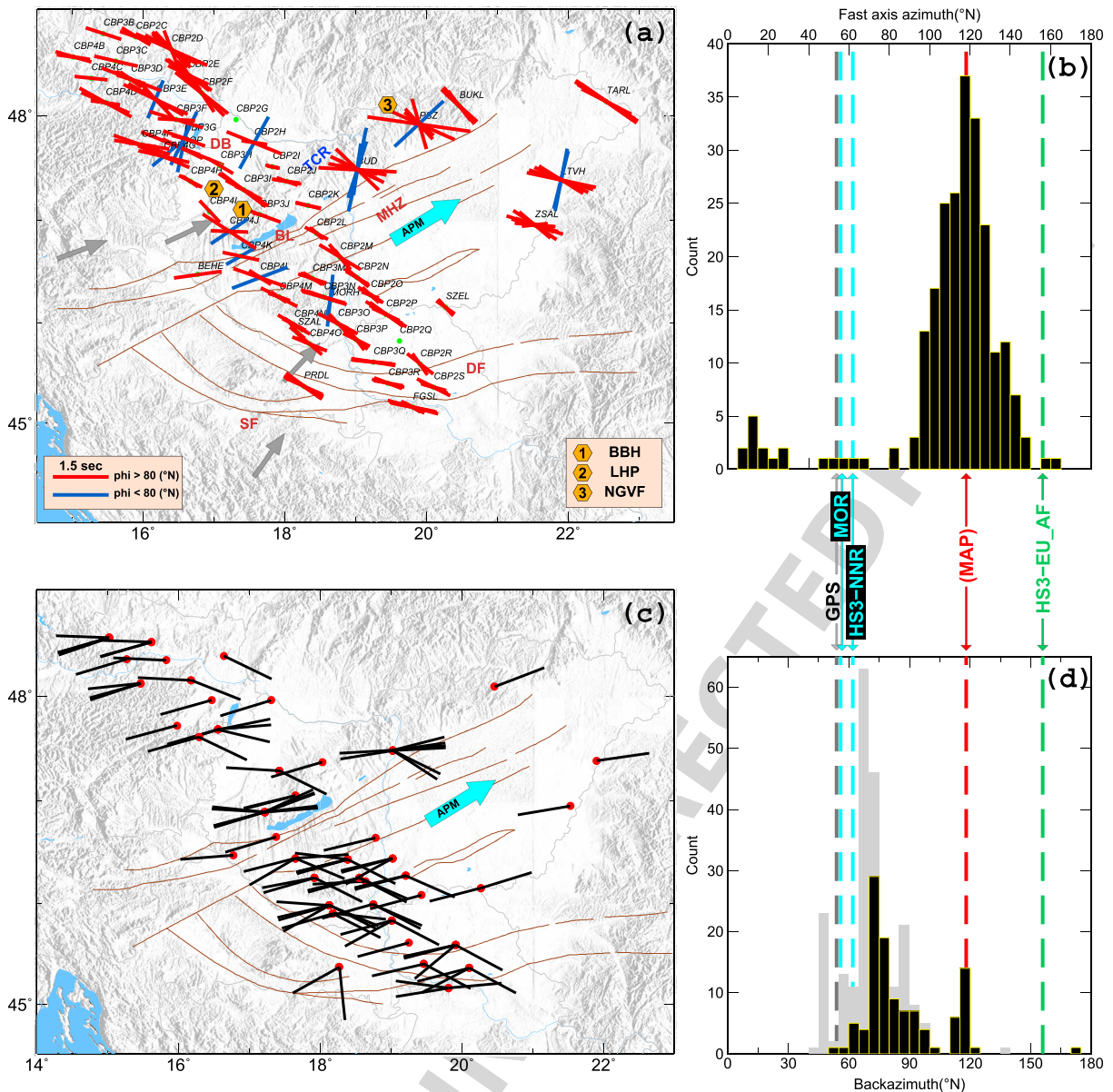


Figure 2. (a) Individual measurements of SKS splitting parameters shown at each station. Fast axes with azimuths larger than 80°N are shown in red, and those less than 80°N are colored in blue, according to statistical distribution (histogram in Figure 2b). Brown lines display the major faults in the region. DB: Danube basin, BL: Balaton fault, MHZ: Mid-Hungarian Shear Zone, DF: Drava fault, and SF: Sava fault. Change in the NE-SW fast pattern (blue lines) occurs in the Transdanubian Central Range (TCR, see text). Crustal motion on average of $\sim 54^\circ\text{N}$ based on GPS data [Grenerczy and Kenyeres, 2006] is represented by the small gray arrows. The APM direction is indicated by the cyan arrow ($\sim 59^\circ\text{N}$, an average of MOR (MORVEL2010) and HS3-NNR, see below). The location of xenoliths sample origin is shown by orange symbols; #1: Szentbaekkala, in the Bakony-Balaton Highland, BBH; #2: Little Hungarian Plain, LHP [Kovács et al., 2012]; #3: Nógrád-Gömör Volcanic field, NGVF [Klébesz et al., 2015]. (b) Histogram of the distribution of the fast orientation. The direction of crustal motion (GPS data [Grenerczy and Kenyeres, 2006]) and APMs are also shown in this histogram; MOR: (56°N) based on MORVEL2010 model [DeMets et al., 2010] with respect to Africa reference plate; HS3-NNR: (62°N) based on HS3-Nuvel1A [Gripp and Gordon, 2002] in no-net-rotation; HS3-EU-AF: (156°N) based on HS3-Nuvel1A with respect to Africa reference plate. MAP: major anisotropy pattern ($\sim 120^\circ\text{N}$) observed dominantly in the CPR. (c) Map of the good null measurements. Null orientations are illustrated by lines pointing to the station from the event. (d) Histogram of the distribution of the nulls. Back azimuthal distribution of the fast orientation is also shown in the background (light gray bars).

01
02
03
04
05
06
07
08
09
10
11
12
13
14
15
16
17
18
19
20
21
22
23
24
25
26
27
28
29
30
31
32
33
34
35
36
37
38
39
40
41
42
43
44
45
46
47
48
49
50
51
52
53
54
55

[Kovács *et al.*, 2012]. Since the focus of the present study is on the upper mantle, we used the results of this group. This group is referred to as A-type fabric, in which the fast axis of individual crystals is usually aligned in the direction of shear [e.g., Mainprice *et al.*, 2000]. This provided us with additional constraints on the LPO (Lattice Preferred Orientation) of the upper mantle anisotropic minerals. We therefore applied A-type olivine fabric in our interpretation of the fast azimuth to infer the shear orientation. This group of xenoliths shows high shear wave anisotropy in the range of 5.4–7.3%. This brings a good knowledge of anisotropy magnitude, which, together with the *SK(K)S* splitting delays, makes us able to estimate the thickness of anisotropic layer. The other group of xenoliths—representing the shallower and thin remnants of the lithospheric mantle after the extension—showed relatively weak shear wave anisotropy (3.0–5.3%). Because of the lower degree of anisotropy and very small thickness of this layer (~10 km [see Kovács *et al.*, 2012; Klébesz *et al.*, 2015]), we did not use these data.

4. Results

4.1. *SK(K)S* Splitting Measurements

Good quality individual measurements at each station are presented in Figure 2 and are listed in supporting information Table S1 including the error of measurements. The uncertainty of the fast orientation is mostly less than 20° and delay time error is mainly between 0.1 and 0.3 s (Table S1). Most of the stations depict a robust pattern of fast orientation (e.g., CBP3I, TARL, and CBP2F) that is mainly oriented NW-SE (hereafter major pattern). Figure 2b shows a histogram of the distribution of the fast azimuth where the values greater than 80° N display a nearly normal distribution around an average value of 120°N. The majority of the measurements fall into this distribution, in the range of 85°N to 145°N, while there are a number of good quality measures showing fast azimuths less than 80°N. To represent the individual measurements in a clearer way, they are colored according to their value (of fast orientation azimuth) in red and blue (Figure 2).

In the northwestern part of the Pannonian basin (e.g., CBP4B), the prevailing fast azimuth is ~105°N, while a second pattern of anisotropy (hereafter minor pattern) shows up at ~25°N (Figure 2). At middle latitudes where the Mid-Hungarian Shear Zone (MHZ) is located, the major anisotropy pattern changes from 105° to 120°–130°N, while the minor pattern is ~70°N. The smallest values of splitting delays are observed largely from the stations located at about the megahertz area. In the southern part, where the stations CBP3Q, CBP3R, CBP2S, FGSL, and PRDL are located, the dominant NW-SE fast orientation transitions into ~105°N, similar pattern as in the northwestern part. Notably, they roughly follow the trend of the Drava and Sava faults in this area with an exception at CBP2R (Figure 2a). At three stations CBP2G, CBP3L, and CBP2Q no good splitting measurement was obtained.

At a number of stations, the measurements are neither tightly distributed nor randomly scattered (i.e., CBP3E, CBP3G, CBP4G, CBP4J, CBP4K, CBP4L, CBP2H, MORH, BUD, PSZ, LTVH, and SOP). They show two groups of fast orientation. In such cases, variation of splitting parameters as a function of incoming polarization (event back azimuth for *SK(K)S* phases) could generally be considered as a signature of multilayer or dipping axis of anisotropy [Silver and Savage, 1994]. Among 11 stations showing two groups of fast orientation, BUD, LTVH, PSZ, and SOP do not show back azimuthal variation, while CBP2H, 3E, 3G, 4G, 4J, 4K, and ZSAL do (supporting information Figure S1). Even though the number of measurements representing back azimuthal dependency is limited, we attempted to assess the presence of two-layer anisotropy. Using the expression of Silver and Savage [1994], we tested all possible combinations of splitting parameters for both single stations and for collections of stations. However, no model of two-layer anisotropy could fit the observations. This might be due to the low number of measurements or alternatively due to lateral variation of anisotropy that can effectively influence *SKS* splitting [Chevrot and Montéiller, 2009]. When anisotropic fabric, especially within the lithosphere, varies in scale smaller than the lateral resolution of the *SKS* (Fresnel zone), incoming rays may sample the region of complex anisotropy. This leads to observed apparent splitting parameters that do not fit two-layer model, even though two anisotropic layers might exist.

In order to evaluate the relation between the observed anisotropy and the motion occurring at the upper mantle scale, we compared the fast orientations with absolute plate motion (APM) and crustal motion from GPS data [Grenerczy and Kenyeres, 2006]. We used the APM directions derived by different models and references. MORVEL2010 [DeMets *et al.*, 2010] in both African plate reference and no-net-rotation (NNR), and HS3-Nuvel1A [Gripp and Gordon, 2002] in NNR yield APM between 56° and 62°N, while the HS3-Nuvel1A model in Africa reference gives APM of 156°N (Figure 2). The most striking feature is that the major anisotropy pattern (~120°N) correlates neither with APM directions nor with the direction of crustal motion.

Table 1. List of Stations With the Average Value of Fast Orientations and Splitting Delays Including Their Corresponding Error

Station	Net	Longitude	Latitude	ϕ (deg)	ϕ -err	δt (s)	δt -err	SM	GS	NM	GN	Station	Net	Longitude	Latitude	ϕ (deg)	ϕ -err	δt (s)	δt -err	SM	GS	NM	GN
BEHE	HU	16.77	46.47	82	-	1.30	-	8	1	1	1	CBP3G	YG	16.58	47.78	107	2	0.80	0.33	6	4	0	0
BUD	HU	19.02	47.48	111	9	1.46	0.26	23	11	13	8	CBP3G				26	-	1.60	-	3			
BUD				14	4	1.45	0.63	4				CBP3H	YG	17.09	47.52	121	-	0.80	-	3	1	0	0
LTVH	HU	21.90	47.38	110	6	1.62	0.18	12	5	2	1	CBP3I	YG	17.42	47.29	120	5	1.17	0.42	6	4	2	2
LTVH				13	2	1.65	0.07	2				CBP3J	YG	17.65	47.05	108	3	0.80	0.55	2	2	2	2
MORH	HU	18.64	46.21	10	5	1.10	0.42	3	2	3	1	CBP3L	YG	18.06	46.67	Na		Na		1	0	0	0
PSZ	HU	19.89	47.92	128	19	1.68	0.59	12	5	2	0	CBP3M	YG	18.39	46.43	115	5	0.70	0.07	5	4	6	5
PSZ				47	-	1.80	-	1				CBP3N	YG	18.55	46.25	107	2	1.00	0.27	8	4	5	4
SOP	HU	16.56	47.68	113	3	1.53	0.69	20	3	9	5	CBP3O	YG	18.75	45.99	122	9	0.82	0.22	5	4	3	3
SOP				12	-	1.30	-	1				CBP3P	YG	19.01	45.83	125	9	0.72	0.07	5	5	3	3
BUKL	HU	20.46	48.09	136	3	1.07	0.15	9	7	1	1	CBP3Q	YG	19.25	45.61	94	5	1.05	0.16	5	3	1	1
CBP2C	YG	15.90	48.74	113	5	0.85	0.05	5	4	2	0	CBP3R	YG	19.46	45.40	106	4	0.83	0.04	5	4	2	2
CBP2D	YG	16.40	48.62	130	8	1.32	0.22	14	9	0	0	CBP4B	YG	15.02	48.55	101	4	0.93	0.05	7	3	6	4
CBP2E	YG	16.64	48.38	131	11	1.20	0.20	8	5	1	1	CBP4C	YG	15.27	48.35	96	-	0.90	-	3	1	1	1
CBP2F	YG	16.83	48.21	134	8	1.48	0.27	6	4	1	0	CBP4D	YG	15.47	48.12	109	6	1.04	0.34	6	5	3	3
CBP2G	YG	17.31	47.96	Na		Na		2	0	2	1	CBP4F	YG	15.98	47.72	102	6	1.30	0.40	4	3	3	1
CBP2H	YG	17.57	47.74	105	10	1.15	0.62	4	2	1	0	CBP4G	YG	16.29	47.61	138	7	1.45	0.07	5	2	3	2
CBP2H				29	-	1.60	-	1				CBP4G				50	-	0.80	-	1			
CBP2I	YG	17.83	47.51	102	2	0.35	0.07	4	2	0	0	CBP4H	YG	16.67	47.37	120	4	0.60	0.09	3	3	0	0
CBP2J	YG	18.03	47.37	103	6	0.70	0.09	4	3	2	1	CBP4I	YG	16.94	47.08	137	-	0.80	-	3	3	0	0
CBP2K	YG	18.33	47.14	103	1	0.70	0.00	3	2	0	0	CBP4J	YG	17.22	46.89	138	21	1.35	0.48	3	2	11	9
CBP2L	YG	18.45	46.87	127	8	0.53	0.14	3	3	0	0	CBP4J				56	-	1.20	-	1			
CBP2M	YG	18.78	46.64	135	7	0.82	0.24	9	5	2	1	CBP4K	YG	17.38	46.65	102	-	1.00	-	3	1	2	1
CBP2N	YG	19.02	46.44	125	3	0.72	0.07	8	5	5	3	CBP4K				60	-	0.90	-	1			
CBP2O	YG	19.21	46.27	123	6	0.63	0.09	9	6	3	3	CBP4L	YG	17.65	46.44	116	5	0.85	0.37	7	4	7	4
CBP2P	YG	19.43	46.08	120	3	1.00	0.14	8	6	5	1	CBP4L				69	-	1.60	-	1			
CBP2Q	YG	19.62	45.82	Na		Na		2	0	0	0	CBP4M	YG	17.92	46.25	116	6	0.70	0.23	4	4	4	3
CBP2R	YG	19.91	45.59	136	12	0.80	0.14	7	2	5	4	CBP4N	YG	18.13	45.98	120	2	0.72	0.13	5	5	6	6
CBP2S	YG	20.10	45.36	112	4	0.78	0.12	9	5	4	3	CBP4O	YG	18.35	45.79	119	10	0.90	0.09	5	3	0	0
CBP3B	YG	15.44	48.77	108	-	1.00	-	1	1	0	0	FGSL	YG	19.81	45.16	109	7	1.02	0.31	7	5	3	3
CBP3C	YG	15.62	48.51	103	-	1.20	-	15	11	1	1	PRDL	YG	18.27	45.37	120	5	1.15	0.05	4	4	4	2
CBP3D	YG	15.83	48.34	116	3	0.80	0.19	15	11	1	1	SZAL	YG	18.18	45.90	133	7	0.57	0.11	3	3	4	3
CBP3E	YG	16.18	48.15	126	7	1.30	0.42	6	5	3	2	SZEL	YG	20.27	46.15	132	9	0.60	0.00	5	2	2	2
CBP3E				22	-	1.10	-	1				TARL	YG	22.54	48.13	122	2	1.65	0.17	14	10	0	0
CBP3F	YG	16.47	47.96	100	10	1.25	0.35	5	2	1	1	ZSAL	YG	21.53	46.95	106	10	1.16	0.18	9	8	2	1

^aFor the stations showing two patterns of fast orientation, two average values are presented (group average). The dash symbol for the error indicates only one good measurement obtained at the station. "Na" represents no good quality measurement. Number of splitting measurements (SM) and good quality splitting (GS) are listed together with the number of null measurements (NM) and good quality null (GN).

On the other hand, APM at about 60° and crustal motion agree with the fault trends in the Mid-Hungarian Shear Zone (Figure 2), which is more or less similar to the minor pattern of anisotropy (NE-SW) observed at the three stations CBP4J, CBP4K, and CBP4L. Farther to the northwest, the NE-SW fast orientation shows a counterclockwise rotation (Figure 2). This change occurs in the area where the Transdanubian Central Range is located (small mountain chain to the north of the Balaton fault, Figures 1 and 2). It seems that the NE-SW anisotropy (minor pattern) may have been affected by small-scale orogeny and shear zones in this area.

We also compared the null measurements with the APM directions and GPS data. Generally, null orientations are observed 90° apart, invoking fast and slow polarization azimuth [Silver and Chan, 1991; Barruol and Souriau, 1995; Savage, 1999]. A histogram of our null measurements shows two peaks which are 40–50° apart.

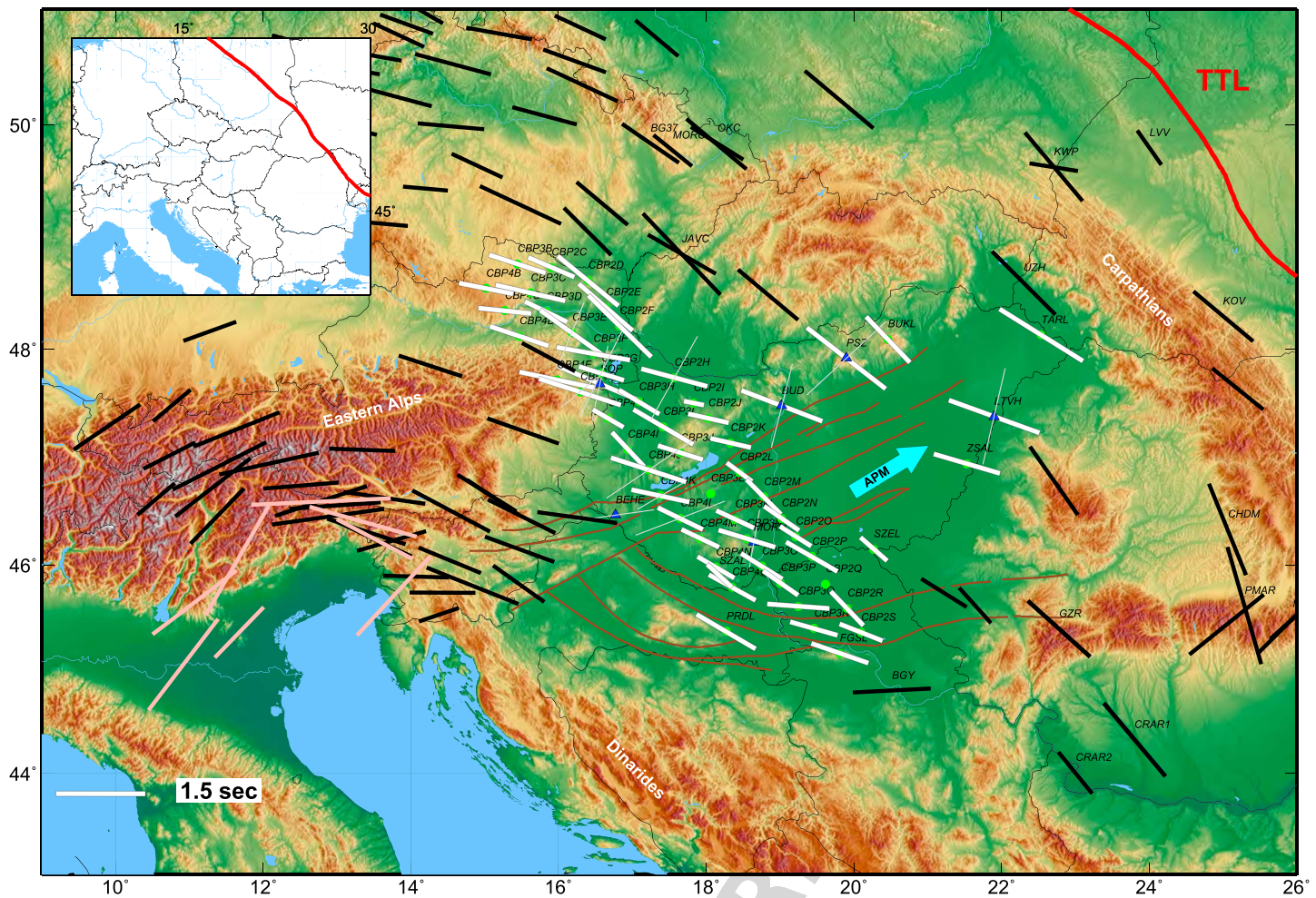


Figure 3. Average shear wave splitting parameters, calculated over the good quality measures at each station. Orientation of the bars represents the fast axis azimuth ($^{\circ}$ N), and their lengths correspond to the splitting delay time in seconds. White bars are the results of this study. Data from previous SKS splitting studies [Wiejacz, 2001; Ivan et al., 2008; Plomerova et al., 2012; Vecsey et al., 2014; Qorbani et al., 2015], are shown by black bars. Thin gray bars display the minor average values at some stations (see text). The red line shows the Tornquist-Teisseyre line (TTL). The arrow shows absolute plate motion (APM) direction (see Figure 2). Inset shows the extension of the TTL in a larger view of Europe. Brown lines display the major faults in the region. Results from Salimbeni et al. [2013] are shown in different color (pink) in order to see the effect of inward flow into the Pannonian basin (see text).

The peak at about 120° N corresponds to the dominant NW-SE fast orientation. However, the second peak at 75° N does not agree with neither the fast nor the slow orientation (Figure 2). It is neither in line with the APM and crustal motion. The back azimuthal distribution of the fast orientation (shown in the background of the null histogram) shows more or less the same distribution as the nulls. This may be an effect of the complexity of the recorded seismic signal, e.g., due to complex structures under the stations, in turn, leading to a lower signal-to-noise ratio; then sometimes no splitting measurements are possible even for favorable back azimuths.

4.2. Overall Pattern of Anisotropy

The overall anisotropy pattern is generally estimated by averaging the individual measurements. Here the average splitting parameters are presented, applying circular and linear averaging over the fast azimuth and splitting delays, respectively. Care should be taken since simply making an average over all measurements may not represent the anisotropic structure below the station (misaveraging effect). We therefore apply group averaging for stations depicting two groups of fast orientations. We determined an average for each group of measurements showing close fast orientation based on the statistical distribution shown in Figure 2. In particular, for the stations with two patterns of anisotropy (NW-SE and NE-SW), two averages are presented. The station average values are listed in Table 1, including the averaging error (95% confidence interval).

01
02
03
04
05
06
07
08
09
10
11
12
13
14
15
16
17
18
19
20
21
22
23
24
25
26
27
28
29
30
31
32
33
34
35
36
37
38
39
40
41
42
43
44
45
46
47
48
49
50
51
52
53
54
55

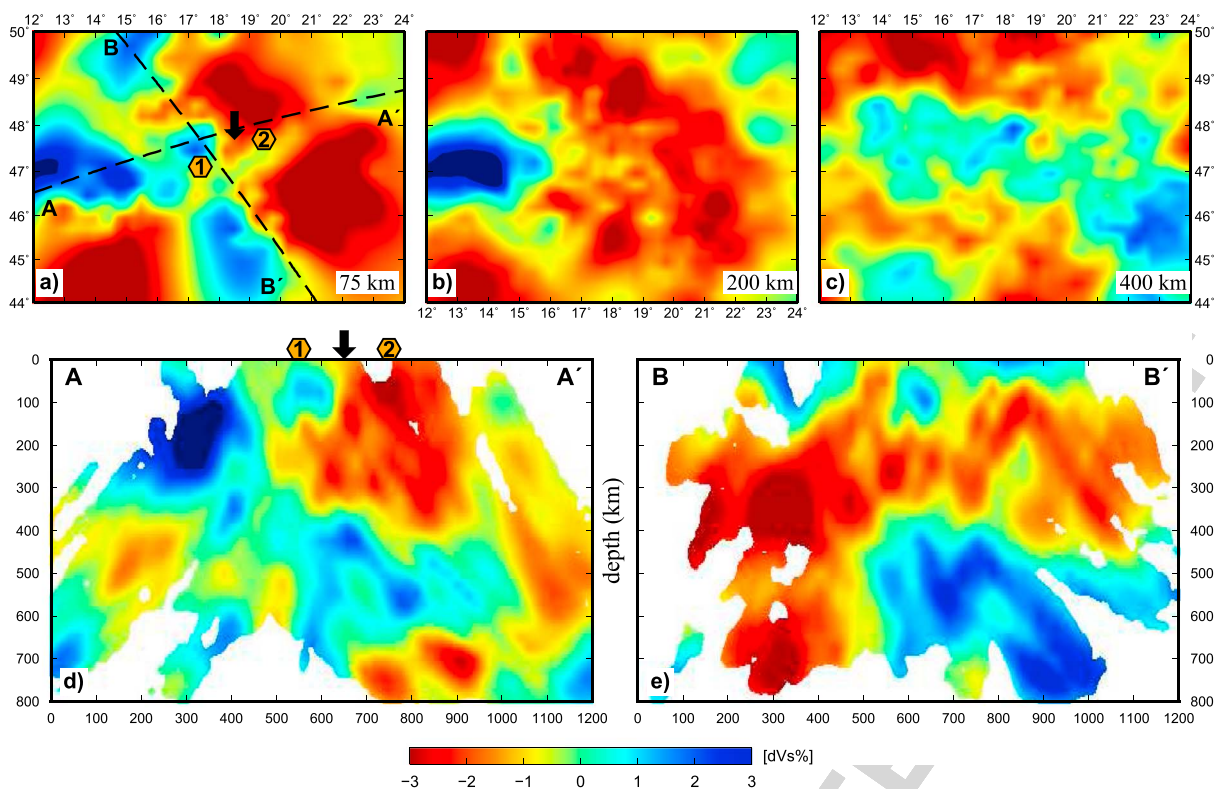


Figure 4. Figures 4a–4c show shear wave velocity anomalies [Dando *et al.*, 2011] shown at the three depth slices, 75, 200, and 400 km. (a) The origin of xenolith sample is represented by hexagons, #1 for BBH and #2 for NGVF. The surface positions of two vertical profiles, AA', BB', are also traced. (b) At 200 km depth the large area of low-velocity zone is notable. (c) At 400 km depth, a broad region of high-velocity anomaly (interpreted as a possible slab graveyard) can be seen extending to the mantle transition zone. Figures 4d and 4e show two vertical profiles of the velocity model. (d) AA' profile. The origin of the xenolith samples is also shown on this profile. Note the changing thickness of the low-velocity zone underneath. (e) NW-SE vertical profile, BB', shows a layer of low-velocity zone between 100 and 400 km depth which is suggested as the source of the NW-SE anisotropy. The scale of *S* wave velocity anomaly (%) is the same for all figures.

Figure 3 shows the average splitting parameters, where the dominant fast azimuth for the entire CPR is NW-SE. In Figure 3, our results are shown together with the former *SKS* splitting measurements in the surrounding regions. The dominant fast orientation is coherent with these results. To the north, in the Bohemian Massif [Plomerova *et al.*, 2012; Vecsey *et al.*, 2014] the fast orientation is NW-SE as well as near the Tornquist-Teisseyre zone in Poland [Wiejacz, 2001]. To the southeast, in the Apuseni area (Figure 1), and in the South Carpathians in Romania, *SKS* splitting results [Ivan *et al.*, 2008] agree with what we observed (Figure 3). The source-side *S* wave splitting data [Russo and Mocanu, 2009], those sampling the East and South Carpathians, also show similar fast orientation as our measurements. This agreement is valid until the eastern part of the Eastern Alps [Qorbani *et al.*, 2015], where the overall anisotropy eventually changes from NW-SE to NE-SW in the central Alps (~ 12°E, Figure 3). A similar change has also been observed in the Southern Alps and north Dinarides, to the west and east of 12° E [Salimbeni *et al.*, 2013, Figure 3]. On the northwestern part of the CBP profiles (e.g., CBP4B station), the NW-SE fast orientation slightly rotates to WNW-ESE, following the large-scale rotating deformation pattern, which has already been observed along the Alps [Bokelmann *et al.*, 2013].

4.3. Local Variation of Anisotropy

Beyond the dominant NW-SE oriented deformation pattern, fast axis orientations and splitting delay times show some small-scale spatial variations. The delay times show unusually low values particularly in a region between the Danube basin and the megahertz (Figure 2, e.g., CBP2I, -2 J, -2 K). In contrast, we observed large values at the nearby stations (e.g., PSZ and BUD), where an abrupt change in the delay time (60%) occurs from station CBP2K to BUD (Figure 2).

In order to assess the relation between the delay times and geometry (thickness) of anisotropic structure, we compared our results to tomographic images. Figure 4 shows *S* wave velocity variations derived from the CBP data [Dando *et al.*, 2011]. The low-velocity zone—generally interpreted as hot and viscous asthenospheric material which can flow—can be identified in the depth extent between 75 and 400 km from the depth slices

and the two vertical profiles in the figure. The thickness of the low-velocity zone is dramatically increased from the west to the east (along the AA' profile, marked by the arrow in Figure 4). This change occurs in the same area where the transition from small to large delay times appears. It suggests that the low-velocity zone (as an anisotropic layer) under the CBP2J is thin; thus, it can cause small splitting delay, and vice versa for the BUD station.

Additionally, we benefited from petrofabric data [Kovács *et al.*, 2012; Klébesz *et al.*, 2015]. Klébesz *et al.* [2015] assessed different foliation and lineation settings for eight xenolith samples taken from the NGVF area (Figure 2) in order to calculate the shear wave anisotropy and to estimate the thickness of upper mantle anisotropy. They compared their results with those from the BBH xenoliths [Kovács *et al.*, 2012]. The comparison showed that for a similar foliation and lineation geometry, the thickness of the anisotropic layer beneath the NGVF should be about twice as much as the layer thickness beneath the BBH. This agrees well with our splitting data. The BBH and NGVF are located in the area where we observed small (~ 0.7 s) and large delay time (~ 1.4 s) respectively, corresponding to the thin and thick low-velocity zone.

5. Discussion

5.1. Role of Crust/Lithosphere

Horváth *et al.* [2006] compiled a crustal map for the CPR, with thicknesses between 25 and 32 km, reaching to 35 km under the Transylvanian basin (Figure 1). Analysis of receiver functions has also shown values of 25–30 km crustal depth, which increases away from the Pannonian basin to the surrounding mountain chains [Hetényi *et al.*, 2015]. The core phases (SKS) used in this study have a dominant period of 10 s (wavelength of approximately 50 km) sensitive to structures of much larger scale [Barruol *et al.*, 2011] than crustal depth in the CPR. Furthermore, crustal anisotropy (due to sedimentary layering, fractures and cracks, and mineral preferred orientation of rocks) generally have an effect on shear wave splitting as 0.1 s per 10 km [Barruol and Mainprice, 1993; Silver, 1996]. This would lead to a delay time in order of 0.2–0.3 s due to anisotropy within the crust in the CPR which is clearly smaller than the mean value of the delay times (~ 1 s) that we observed.

Lithospheric thickness under the Pannonian basin (derived from multiple geophysical studies) is estimated at about ~ 60 km [Horváth, 1993; Posgay *et al.*, 1995; Tari *et al.*, 1999; Horváth *et al.*, 2006]. Assuming single-layer of anisotropy, the thickness of anisotropic layer (D) can be estimated using anisotropy magnitude from petrofabric data (δv), SKS splitting delay time (δt), and shear wave velocity (v_s), as $D = v_s \delta t / \delta v$. Taking 5% anisotropy magnitude (from the xenolith samples) into account together with the mean delay time of 1 s would correspond to a thickness of 100 km that is larger than the average 60 km thickness of the lithosphere. More specifically, the lithosphere-asthenosphere boundary (LAB) under BUD station from receiver functions analysis is at about 70 km depth. Considering a maximum 3.7% anisotropy magnitude from the xenolith samples (NGVF) [Klébesz *et al.*, 2015], and 1.5 s delay time measured at the BUD station, would result in ~ 200 km thickness for the anisotropic layer. This is more than twice the size of the lithosphere (LAB depth) under this station, indicating that the lithosphere alone might not be thick enough to create the observed delay time.

5.2. Asthenospheric Mantle Anisotropy

It has been widely suggested that localized anisotropy in correlation with the surface geology and crustal deformation refers to lithospheric origin, whereas a uniform anisotropy pattern on a large-scale strongly indicates asthenospheric sources [Savage, 1999; Fontaine *et al.*, 2007]. Dominant fast axis orientation under the Eastern Alps, Pannonian basin, Carpathians, Dinarides, Moesian platform, and also southern Bohemian is NW-SE (Figure 3). This large-scale anisotropy is uniformly distributed from the Tauern Window (in the Alps, $\sim 12^\circ$ E) to the Eastern Carpathians, implying that the anisotropy is independent of the orogenic processes, variations in geology, and topography. This also reveals that the correlation length of anisotropy is larger than geological units and tectonic blocks such as the Alcapa and Tisza-Dacia. Although these two units have undergone strong internal deformation in a different manner, the deformation pattern reflected in seismic anisotropy is much simpler. We therefore suggest that the NW-SE fast orientation has originated from asthenospheric deformation (flow/alignment). This suggestion agrees well with the azimuthal anisotropy model previously presented by Zhu and Tromp [2013]. They showed that maximum (peak to peak) anisotropy under the Pannonian basin occurs at 150 km depth which is obviously below the LAB (~ 60 km), and within the asthenospheric mantle.

However, it is not possible to completely exclude the role of the lithosphere on anisotropy. Correspondence of NE-SW fast orientation (minor pattern) with crustal motion, and APM would argue for a contribution of

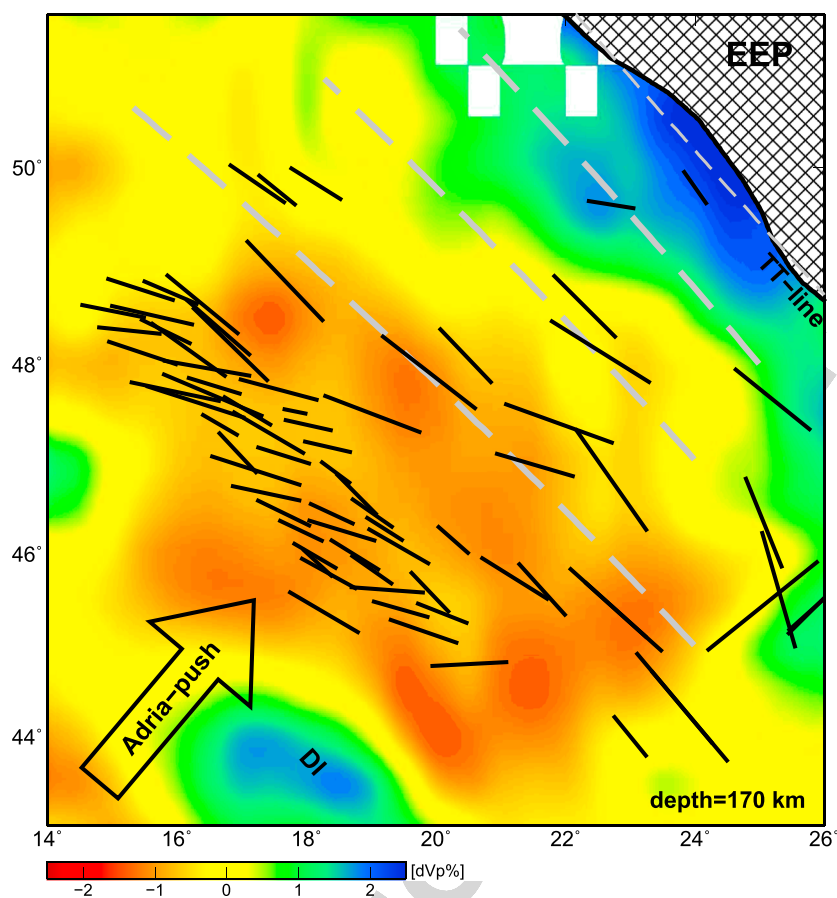


Figure 5. A representative model which is suggested in this study for the anisotropy and deformation under the Carpathian-Pannonian Region. The compressional tectonic regime associated with the northeastward Adria push [Bada *et al.*, 2007; Bus *et al.*, 2009] yields transpressional deformation with a NW-SE shear orientation. *P* wave velocity anomaly at 170 km depth [Koulakov *et al.*, 2009] is shown in the background. The low-velocity zone at this depth is situated between two high-velocity areas (in blue) referring to the presence of cold lithosphere at this depth. EEP: East European platform (EEP) and DI: Dinarides. Dashed lines are lines parallel to the Tornquist-Teisseyre (TT) line, shown by the thick black line. Our average *SKS* splitting results are illustrated by black bars. They are oriented roughly parallel to these lines. TT line is shown by the thick black line.

lithospheric deformation to anisotropy. As crust/lithospheric blocks moves, the shear may align rock crystals parallel to the shear direction. Therefore, even though we could not fit any two-layer model, it seems that the motion of the crust/lithospheric blocks might have a consequence on the observed anisotropy.

Another possible scenario that might explain the NE-SW anisotropy is a northeastward flow under the northern Dinarides [Horváth and Faccenna, 2011]. Tomographic models show a slab gap under the northern Dinarides, near to the Eastern Alps [e.g., Piromallo and Morelli, 2003; Koulakov *et al.*, 2009] (can be seen in Figure 5 between latitudes 44° and 46°). Asthenospheric material may thus flow northeastward into this slab window toward the Pannonian basin [Horváth and Faccenna, 2011]. Such flow could affect the shear wave splitting and might show up as NE-SW fast orientation similar to what we observed at some stations. In this area, *SKS* splitting data derived from a number of Slovenian seismic stations [Qorbani *et al.*, 2015, Figure 3], and near to the Adriatic coast [Salimbeni *et al.*, 2013, Figure 3] depict a slightly complex anisotropy pattern. This can be due to the meeting of a northeastward flow and the NW-SE asthenospheric alignment under the Eastern Alps and the CPR. However, origin of the NE-SW anisotropy is not yet clear and other possible explanations may exist. Further anisotropy measurements and analyses particularly in northern Bosnia and Croatia would be required to elucidate this flow through the slab window into the CPR.

5.3. Eastward Extrusion of the Alcapa Block

Lateral escape of the Alcapa block is an important aspect in investigating lithospheric-asthenospheric deformation and motion. The Alcapa block (Figure 1) is extruding laterally with a tendency to ENE direction as a result of continental collision between Adria and Europe [Ratschbacher et al., 1991a; Fodor et al., 1999; Schmid et al., 2008]. It is still a matter of debate, whether the extrusion happened only on the scale of the crust or the entire lithosphere. Models invoking gravitational collapse of the Alps suggest that only the upper part of crust takes part in the lateral escape [Ratschbacher et al., 1991a; Ranalli, 1995]. Alternatively, some studies [Kovács et al., 2012; van Gelder et al., 2015] proposed that the extrusion occurs on the scale of the entire lithosphere. Here the NW-SE fast orientation from the asthenospheric flow/alignment clearly differs from the direction of the Alcapa block motion. The difference suggests: (1) the eastward extrusion and the NW-SE fast orientation under the CPR are not caused by the same process; (2) crust/lithosphere and asthenosphere are deformed in different ways; (3) the asthenospheric fabric may have been significantly modified since the end of the basin extension.

5.4. Models for Upper Mantle Deformation

As mentioned previously in section 4.1, inconsistency between APM and present NW-SE anisotropy suggests that a model based on shear induced by plate motion would not explain our anisotropy data set. In order to better understand the relation between tectonic field and induced anisotropy, we consider in the following, the various (sometimes conflicting) models that have been proposed for formation, evolution, and current tectonic stage of the CPR.

Mantle upwelling, as plume, is one of the earliest models suggested for the formation of the Pannonian basin [Stegena et al., 1975; Wilson and Downes, 1992]. In this model an active mantle plume would provide extension driving forces. If we assume that we observe the ascent of a plume in the SKS splitting measurements, the pattern of anisotropy should depict a parabolic flow at the base of the lithosphere as a result of interaction between extension, mantle upwelling, and plate motion [Sleep, 1990; Ito et al., 2014]. Shear wave splitting observations at the Eifel hot spot in Germany are consistent with this prediction [Walker et al., 2005]. However, that observation and also numerical prediction [Ito et al., 2014] differ from our splitting data. The NW-SE anisotropy does not agree with the expected anisotropy (parabolic pattern) from a mantle upwelling. *Subduction roll back* along the Eastern Carpathians has been suggested as generating suction, affecting on both the lithosphere and the underlying asthenosphere in a direction perpendicular to the trench. Since the former trench may have been roughly NW-SE oriented (i.e., parallel to the strike of the present-day Eastern Carpathians), slab suction could generate NE-SW oriented flow, with LPO presumably aligned parallel to the flow direction. This would mean that we should observe asthenospheric anisotropy dominantly in NE-SW orientation, which is different from our observations. Houseman and Gemmer [2007] proposed *gravitational instability* of lithospheric mantle as the governing force of the extension of the Pannonian basin. According to this model, the thickened, cold, and dense continental crust/lithosphere may have potential to sink. As unstable lithosphere is downwelling, the developed space is filled and replaced by hot and viscous material from the asthenosphere. This hypothesis could explain the existence of a high-velocity body under the Eastern Alps and western Pannonian, connecting to the slab graveyard [Dando et al., 2011; Ren et al., 2012]. As the flow of the material potentially influences the arrangement of crystallographic orientation of minerals, the direction of replacement may show up in the anisotropy observations. However, since we do not know from which direction such a replacement flow would have arrived, we can only state that it would have needed to come from NW and SE to explain the observed NW-SE fast orientation. Several recent studies emphasized the potential role of relatively young (i.e., Cenozoic) *asthenospheric flow* in association with formation of the Pannonian basin. Kovács et al. [2012] suggested that an active asthenospheric flow was produced as the consequence of collision in the Alps, where asthenospheric material trapped between the colliding continental blocks (i.e., Adria and Europe) most likely escaped perpendicular to the axis of convergence. This would imply WNW-ESE and W-E direction, which is somewhat different from the observed NW-SE anisotropy.

Each model has its pros and cons and as has been noted; it seems our anisotropic measurements (especially NW-SE fast orientation) do not correspond with the above models. The present anisotropy pattern may have been a consequence of recent tectonic events, which might have completely or partially overprinted prior fabrics. In accordance, some studies suggested a tectonic inversion phase for the current stage of the Pannonian basin [Horváth et al., 2006; Bada et al., 2007]. Folding and thrusting, Quaternary uplift and subsidence, and changes in the regional stress field [Ziegler and Dèzes, 2006] support this distinct transition from extension in the Miocene to compression in the Pliocene. Recent GPS data in the northern part of the Dinarides have

given a motion toward the northeast in a rate of 2–3 mm/yr [Grenerczy and Kenyeres, 2006; Bus et al., 2009]. Numerical modeling of the stress field has also suggested that the ongoing indentation of the Adria is the essential local force of the present-day NE-SW compression in the Pannonian basin [Bada et al., 2007].

We argue that the current tectonic inversion phase could contribute to the observed deformation pattern within the upper mantle. The inversion phase would require a compressional tectonic regime acting in the NE-SW orientation, which generally leads to large folding within a weakened crust and lithosphere [Dombrádi et al., 2010]. However, within the viscous asthenosphere, deformation accompanying (oblique) compression is transpression, with deformation styles between the two end-member deformation models of “pure shear” and “simple shear.” It is well documented that dislocation creep mechanism induced by both styles of shear within the asthenosphere results in olivine alignments in which the a axis lies parallel to the shear orientation and normal to the compression, known as A-type fabric [e.g., Tommasi et al., 1999]. The LPO of the xenolith samples taken from the CPR show an A-type fabric of olivine. Therefore, we suggest that the NW-SE anisotropy could potentially be a consequence of compression in a convergent system. The compression is most likely (locally) derived by the Adria plate (Adria push) toward the NE [Bada et al., 2007; Bus et al., 2009]. As the Adria pushes, the asthenospheric material between the Adria (to the west) and East European platform (to the east) are squeezed, resulting in alignments normal to the compression direction. This scenario is proposed as a possible model for the upper mantle deformation mechanism (Adria-East European Compression model, AEEC) under the Carpathian-Pannonian Region. However, enough stress and a long enough time may be needed to completely rearrange the orientation of LPO of olivine in the upper mantle.

The East European platform (EEP) is an old, large and relatively stable plate. It seems natural to consider the EEP as the backstop of the NE convergence acting nearly perpendicular to the edge of the EEP. The border between EEP and western Europe is identified as the Tornquist-Teisseyre line (TTL, Figure 3). Tomographic models show a low-velocity zone between 100 and 400 km depth [e.g., Dando et al., 2011] in the west of the TTL, indicating a relatively thick asthenosphere (Figure 4) beneath a thin lithosphere. Under the EEP itself velocity structures sharply differ from the western part and show a very thick lithosphere (> 250 km) [Koulakov et al., 2009; Ren et al., 2012]. The lithospheric root is thus thick and rigid enough to act against the compression on the scale of the upper mantle. This limits the transpression in the region between the EEP and Adria and forces the material within the asthenosphere to be aligned normal to the compression direction and tends to follow the geometry of the barrier (EEP). To test this, we show parallel lines to (the line best fitting) the TTL in Figure 4, suggesting that this orientation explains a fair number of the shear wave splitting observations. Besides this first-order feature in the observed anisotropy, the pattern shows small deviations from the general trend of the TTL, particularly for the observations in the northwest of the CBP profile, which are located at some distance from the EEP.

6. Conclusion

We have investigated SKS splitting from data recorded by the Carpathian Basin Project (CBP) and permanent stations in the Carpathian-Pannonian Region (CPR). Our results have shown a pattern of upper mantle deformation with prevailing NW-SE fast orientation, which extends under the entire CPR. In comparison to the complex geology and crustal/lithospheric features, this anisotropy suggests a simple deformation pattern. The NW-SE fast orientation is clearly uncorrelated to geological indicators such as the trend of mountain chains, suggesting that the anisotropy most likely has an asthenospheric mantle origin as flow/alignment in NW-SE orientation. This anisotropy is remarkably oblique to the lateral (eastward) movement of the Alcapa block, which suggests that the crust (possibly the lithosphere) and asthenosphere are deformed differently. We observed a few measurements (especially near the Mid-Hungarian Shear Zone) with fast orientation (NE-SW) subparallel to the shear zone. Although difficult to explain with classical one- or two-layer anisotropic models, this may suggest an additional contribution of the lithosphere to the observed anisotropy. The NE-SW anisotropy might also correspond to a northeastward asthenospheric flow through the slab gap under the northern Dinarides. However, this intriguing feature, parallel to the direction of the lateral escape of the Alcapa block, should be studied in more detail, with a higher resolution experiment. Most recent tectonics of the CPR has been suggested to be mainly governed by northeastward push of the Adria in an inversion tectonic phase. We used this expression to propose a model, Adria-East European Compression (AEEC), explaining the NW-SE anisotropy at the asthenospheric mantle depth. According to this model, the asthenospheric material is subjected to an oblique compression due to northeastward pushing of the Adria microplate. This results in mineral alignment normal to compression. The East European platform (EEP) has an important role

in this model. It acts as a backstop in the system and forces the minerals to be aligned with its western margin (i.e., Tornquist-Teisseyre line). This invokes a strong association of the deep deformation with the EEP and the geometry of the Tornquist-Teisseyre line.

Acknowledgments

We thank Greg Houseman and Graham Stuart for the access to the Carpathian Basin Project (CBP) data used in this study. Data were provided through the IRIS Data Management Center, <http://ds.iris.edu/ds/nodes/dmc/>; they are available by contacting Greg Houseman at G.A.Houseman@leeds.ac.uk. We acknowledge the Hungarian Seismological Network as the source of permanent station data, provided (and available) through the GFZ webdc data center, <http://eida.gfz-potsdam.de/webdc3/>. We also thank Ben Dando for preparing the tomography velocity model and M.T. Apoloner for digitizing the fault map. This work was supported by the Austrian Science Fund (FWF) through projects 26391 and 24218. We thank C. Szabó, T. Fancsik, and J. Kiss for discussions. I.K. acknowledges the Bolyai Postdoctoral Fellowship for financial support.

References

- Bada, G., F. Horváth, P. Dövényi, P. Szafián, G. Windhoffer, and S. Cloetingh (2007), Present-day stress field and tectonic inversion in the Pannonian basin, *Global Planet. Change*, *58*(1–4), 165–180, doi:10.1016/j.gloplacha.2007.01.007.
- Barruol, G., and D. Mainprice (1993), A quantitative evaluation of the contribution of crustal rocks to the shear-wave splitting of teleseismic SKS waves, *Phys. Earth Planet. Inter.*, *78*(3–4), 281–300, doi:10.1016/0031-9201(93)90161-2.
- Barruol, G., and A. Souriau (1995), Anisotropy beneath the Pyrenees range from teleseismic shear wave splitting, *Geophys. Res. Lett.*, *22*(4), 493–496, doi:10.1029/94GL03225.
- Barruol, G., P. Silver, and A. Vauchez (1997), Seismic anisotropy in the eastern United States: Deep structure of a complex continental plate, *J. Geophys. Res.*, *102*(B4), 8329–8348.
- Barruol, G., M. Bonnin, H. Pedersen, G. Bokelmann, and C. Tiberi (2011), Belt-parallel mantle flow beneath a halted continental collision: The western Alps, *Earth Planet. Sci. Lett.*, *302*, 429–438, doi:10.1016/j.epsl.2010.12.040.
- Bokelmann, G., E. Qorbani, and I. Bianchi (2013), Seismic anisotropy and large-scale deformation of the Eastern Alps, *Earth Planet. Sci. Lett.*, *383*, 1–6, doi:10.1016/j.epsl.2013.09.019.
- Bowman, J. R., and M. Ando (1987), Shear-wave splitting in the upper-mantle wedge above the Tonga subduction zone, *Geophys. J. R. Astron. Soc.*, *88*(1), 25–41, doi:10.1111/j.1365-246X.1987.tb01367.x.
- Bus, Z., G. Grenczy, L. Táoth, and P. Máonus (2009), Active crustal deformation in two seismogenic zones of the Pannonian region—GPS versus seismological observations, *Tectonophysics*, *474*, 343–352, doi:10.1016/j.tecto.2009.02.045.
- Chevrot, S., and V. Monteiller (2009), Principles of vectorial tomography—The effects of model parametrization and regularization in tomographic imaging of seismic anisotropy, *Geophys. J. Int.*, *179*(3), 1726–1736, doi:10.1111/j.1365-246X.2009.04370.x.
- Dando, B. D. E., G. W. Stuart, G. A. Houseman, E. Hegedüs, E. Brückl, and S. Radovanovic (2011), Teleseismic tomography of the mantle in the Carpathian–Pannonian region of central Europe, *Geophys. J. Int.*, *186*(1), 11–31, doi:10.1111/j.1365-246X.2011.04998.x.
- DeMets, C., R. G. Gordon, and D. F. Argus (2010), Geologically current plate motions, *Geophys. J. Int.*, *181*(1), 1–80.
- Dombbrádi, E., D. Sokoutis, G. Bada, S. Cloetingh, and F. Horváth (2010), Modelling recent deformation of the Pannonian lithosphere: Lithospheric folding and tectonic topography, *Tectonophysics*, *484*(1), 103–118.
- Fodor, L., L. Csontos, G. Bada, I. Györfi, and L. Benkovic (1999), Tertiary tectonic evolution of the Pannonian Basin system and neighbouring orogens: A new synthesis of palaeostress data, *Geol. Soc. London Spec. Publ.*, *156*(1), 295–334.
- Fontaine, F. R., G. Barruol, A. Tommasi, and G. H. R. Bokelmann (2007), Upper-mantle flow beneath French Polynesia from shear wave splitting, *Geophys. J. Int.*, *170*(3), 1262–1288, doi:10.1111/j.1365-246X.2007.03475.x.
- Fouch, M., and S. Rondenay (2006), Seismic anisotropy beneath stable continental interiors, *Phys. Earth Planet. Inter.*, *158*, 292–320.
- Grenczy, G., and A. Kenyeres (2006), *The Adria Microplate: GPS Geodesy, Tectonics and Hazards*, Springer, chap. Crustal deformation between Adria and the European platform from space geodesy, 321–334 pp., Netherlands, Dordrecht.
- Gripp, A. E., and R. G. Gordon (2002), Young tracks of hotspots and current plate velocities, *Geophys. J. Int.*, *150*(2), 321–361, doi:10.1046/j.1365-246X.2002.01627.x.
- Haas, J., P. Mioč, J. Pamić, B. Tomljenović, P. Árkai, A. Bérczi-Makk, B. Koroknai, S. Kovács, and E. Rálich-Felgenhauer (2000), Complex structural pattern of the Alpine–Dinaridic–Pannonian triple junction, *Int. J. Earth Sci.*, *89*(2), 377–389.
- Hetényi, G., Y. Ren, B. Dando, G. W. Stuart, E. Hegedüs, A. C. Kovács, and G. A. Houseman (2015), Crustal structure of the Pannonian Basin: The AlCaPa and Tisza terrains and the mid-Hungarian zone, *Tectonophysics*, *646*, 106–116.
- Horváth, F., G. Bada, P. Szafián, G. Tari, A. Adáám, and S. Cloetingh (2006), Formation and deformation of the Pannonian Basin: Constraints from observational data, *Geol. Soc. London, Mem.*, *32*(1), 191–206, doi:10.1144/GSL.MEM.2006.032.01.11.
- Horváth, F., B. Musitz, A. Balázs, A. Váegh, A. Uhrin, A. Nádor, B. Koroknai, N. Pap, T. Táoth, and G. Wáorum (2015), Evolution of the Pannonian basin and its geothermal resources, *Geothermics*, *53*, 328–352, doi:10.1016/j.geothermics.2014.07.009.
- Horváth, F. (1993), Towards a mechanical model for the formation of the Pannonian basin, *Tectonophysics*, *226*(1), 333–357.
- Horváth, F., and C. Faccenna (2011), Understanding extension within a convergent orogen: Initial results on seismic structure from the Carpathian Basins Project, in *EGU General Assembly EGU2011-8894-2*, Vienna, Austria.
- Houseman, G., and G. Stuart (2011), Understanding extension within a convergent orogen: Lithospheric structure of the Pannonian Basin, Scientific Report SEIS-UK loan: 795, NERC Geophysical Equipment Facility.
- Houseman, G. A., and L. Gemmer (2007), Intra-orogenic extension driven by gravitational instability: Carpathian-Pannonian orogeny, *Geology*, *35*(12), 1135–1138, doi:10.1130/G23993A.1.
- Huismans, R. S., Y. Y. Podladchikov, and S. Cloetingh (2001), Dynamic modeling of the transition from passive to active rifting, application to the Pannonian Basin, *Tectonics*, *20*(6), 1021–1039, doi:10.1029/2001TC900010.
- Ito, G., R. Dunn, A. Li, C. J. Wolfe, A. Gallego, and Y. Fu (2014), Seismic anisotropy and shear wave splitting associated with mantle plume-plate interaction, *J. Geophys. Res. Solid Earth*, *119*(6), 4923–4937.
- Ivan, M., M. Popa, and D. Ghica (2008), SKS splitting observed at Romanian broad-band seismic network, *Tectonophysics*, *462*, 89–98, doi:10.1016/j.tecto.2007.12.015.
- Karato, S., H. Jung, I. Katayama, and P. Skemer (2008), Geodynamic significance of seismic anisotropy of the upper mantle: New insights from laboratory studies, *Annu. Rev. Earth Planet. Sci.*, *36*, 59–95, doi:10.1146/annurev.earth.36.031207.124120.
- Klébesz, R., Z. Grácz, G. Szanyi, N. Liptai, I. Kovács, L. Patkó, Z. Pintér, G. Falus, V. Wesztergom, and C. Szabó (2015), Constraints on the thickness and seismic properties of the lithosphere in an extensional setting (Nógrád-Gömör Volcanic Field, Northern Pannonian Basin), *Acta Geod. et Geophysic.*, 1–17, doi:10.1007/s40328-014-0094-0.
- Koulakov, I., M. K. Kaban, M. Tesauro, and S. Cloetingh (2009), P- and S-velocity anomalies in the upper mantle beneath Europe from tomographic inversion of ISC data, *Geophys. J. Int.*, *179*(1), 345–366, doi:10.1111/j.1365-246X.2009.04279.x.
- Kovács, I., G. Falus, G. Stuart, K. Hidas, C. Szabó, M. Flower, E. Hegedüs, K. Posgay, and L. Zilahi-Sebess (2012), Seismic anisotropy and deformation patterns in upper mantle xenoliths from the central Carpathian-Pannonian region: Asthenospheric flow as a driving force for cenozoic extension and extrusion?, *Tectonophysics*, *514-517*, 168–179, doi:10.1016/j.tecto.2011.10.022.
- Long, M., and T. Becker (2010), Mantle dynamics and seismic anisotropy, *Earth Planet. Sci. Lett.*, *297*, 341–354, doi:10.1016/j.epsl.2010.06.036.

- Mainprice, D., G. Barruol, and W. Ben Ismail (2000), The seismic anisotropy of the Earth's mantle: From single crystal to polycrystal, in *Composition, Structure and Dynamics of the Lithosphere–Asthenosphere System*, Geophysical Monograph Series, vol. 117, edited by D. Mainprice, G. Barruol, and W. Ben Ismail, pp. 237–264, AGU, Washington, D. C.
- Márton, E., D. Vass, and I. Tunyi (2000), Counterclockwise rotations of the Neogene rocks in the East Slovak Basin, *Geol. Carpathica Bratislava*, 51(3), 159–168.
- Nicolas, A., F. Boudier, and A. Boullier (1973), Mechanisms of flow in naturally and experimentally deformed peridotites, *Am. J. Sci.*, 273(10), 853–876.
- Piromallo, C., and C. Morelli (2003), P wave tomography of the mantle under the Alpine-Mediterranean area, *J. Geophys. Res.*, 108(B2), 2065, doi:10.1029/2002JB001757.
- Plomerova, J., L. Vecsey, and V. Babuska (2012), Mapping seismic anisotropy of the lithospheric mantle beneath the Northern and Eastern Bohemian Massif (Central Europe), *Tectonophysics*, 564–565, 38–53, doi:10.1016/j.tecto.2011.08.011.
- Posgay, K., T. Bodoky, E. Hegedüs, S. Kovácsvölgyi, L. Lenkey, P. Szafián, E. Takács, Z. Tímár, and G. Varga (1995), Asthenospheric structure beneath a Neogene basin in southeast Hungary, *Tectonophysics*, 252(1–4), 467–484, doi:10.1016/0040-1951(95)00098-4.
- Qorbani, E., I. Bianchi, and G. Bokelmann (2015), Slab detachment under the Eastern Alps seen by seismic anisotropy, *Earth Planet. Sci. Lett.*, 409(0), 96–108, doi:10.1016/j.epsl.2014.10.049.
- Ranalli, G. (1995), *Rheology of the Earth*, Springer Science & Business Media pp., Netherlands.
- Ratschbacher, L., O. Merle, P. Davy, and P. Cobbold (1991a), Lateral extrusion in the eastern Alps. Part I: Boundary conditions and experiments scaled for gravity, *Tectonics*, 10, 245–256, doi:10.1029/90TC02622.
- Ren, Y., G. Stuart, G. Houseman, B. Dando, C. Ionescu, E. Hegedüs, S. Radovanović, and Y. Shen (2012), Upper mantle structures beneath the Carpathian–Pannonian region: Implications for the geodynamics of continental collision, *Earth Planet. Sci. Lett.*, 349–350, 139–152, doi:10.1016/j.epsl.2012.06.037.
- Russo, R., and V. Mocanu (2009), Source-side shear wave splitting and upper mantle flow in the Romanian Carpathians and surroundings, *Earth Planet. Sci. Lett.*, 287(1–2), 205–216, doi:10.1016/j.epsl.2009.08.028.
- Salimbeni, S., S. Pondrelli, and L. Margheriti (2013), Hints on the deformation penetration induced by subductions and collision processes: Seismic anisotropy beneath the Adria region (Central Mediterranean), *J. Geophys. Res.*, 118(11), 5814–5826, doi:10.1002/2013JB010253.
- Savage, M. (1999), Seismic anisotropy and mantle deformation: What have we learned from shear wave splitting?, *Rev. Geophys.*, 37, 65–106.
- Schmid, S., D. Bernoulli, B. Fügenschuh, L. Matenco, S. Schefer, R. Schuster, M. Tischler, and K. Ustaszewski (2008), The Alpine-Carpathian-Dinaridic orogenic system: Correlation and evolution of tectonic units, *Swiss J. Geosci.*, 101(1), 139–183, doi:10.1007/s00015-008-1247-3.
- Silver, P. (1996), Seismic anisotropy beneath the continents: Probing the depths of geology, *Annu. Rev. Earth Planet. Sci.*, 24, 385–432.
- Silver, P. G., and W. Chan (1988), Implications for continental structure and evolution from seismic anisotropy, *Nature*, 335(6185), 34–39, doi:10.1038/335034a0.
- Silver, P. G., and W. W. Chan (1991), Shear wave splitting and subcontinental mantle deformation, *J. Geophys. Res.*, 96(B10), 16,429–16,454.
- Silver, P. G., and M. K. Savage (1994), The interpretation of shear-wave splitting parameters in the presence of two anisotropic layers, *Geophys. J. Int.*, 119(3), 949–963, doi:10.1111/j.1365-246X.1994.tb04027.x.
- Sleep, N. H. (1990), Hotspots and mantle plumes: Some phenomenology, *J. Geophys. Res.*, 95(B5), 6715–6736.
- Stegena, L., B. Geczy, and F. Horváth (1975), Late Cenozoic evolution of the Pannonian basin, *Tectonophysics*, 26(1), 71–90.
- Tari, G., P. Dövényi, I. Dunkl, F. Horváth, L. Lenkey, M. Stefanescu, P. Szafián, and T. Tóth (1999), Lithospheric structure of the Pannonian basin derived from seismic, gravity and geothermal data, *Geol. Soc. London Spec. Publ.*, 156(1), 215–250.
- Tommasi, A., B. Tikoff, and A. Vauchez (1999), Upper mantle tectonics: Three-dimensional deformation, olivine crystallographic fabrics and seismic properties, *Earth Planet. Sci. Lett.*, 168(1–2), 173–186, doi:10.1016/S0012-821X(99)00046-1.
- van Gelder, I., E. Willingshofer, and D. Sokoutis (2015), *Lateral Extrusion of the Upper Plate in Response to Subduction of a Non-rigid Continental Plate: Analogue Modelling and Application to the Eastern Alps*, 12th Alpine Workshop, EGU, Montgenevre / Briançon–French Hautes-Alpes, 56 pp.
- Vauchez, A., A. Tommasi, and D. Mainprice (2012), Faults (shear zones) in the Earth's mantle, *Tectonophysics*, 558–559, 1–27, doi:10.1016/j.tecto.2012.06.006.
- Vecsey, L., J. Plomerová, and V. Babuška (2014), Mantle lithosphere transition from the East European Craton to the Variscan Bohemian Massif imaged by shear-wave splitting, *Solid Earth*, 5(2), 779–792, doi:10.5194/se-5-779-2014.
- Vinnik, L., G. Kosarev, and L. Makeeva (1984), Lithosphere anisotropy from the observation of SKS and SKKS waves, *Doklady Akademii Nauk SSSR*, 278(6), 1335–1339.
- Walker, K. T., G. H. R. Bokelmann, S. L. Klemperer, and G. Bock (2005), Shear-wave splitting around the Eifel hotspot: Evidence for a mantle upwelling, *Geophys. J. Int.*, 163(3), 962–980, doi:10.1111/j.1365-246X.2005.02636.x.
- Wiejacz, P. (2001), Shear wave splitting across Tornquist-Teisseyre zone in Poland, *J. Balkan Geophys. Soc.*, 4(4), 91–100.
- Wilson, M., and H. Downes (1992), Mafic alkaline magmatism associated with the European Cenozoic rift system, *Tectonophysics*, 208(1), 173–182.
- Wüstefeld, A., and G. Bokelmann (2007), Null detection in shear-wave splitting measurements, *Bull. Seismol. Soc. Am.*, 97(4), 1204–1211, doi:10.1785/0120060190.
- Wüstefeld, A., G. Bokelmann, C. Zaroli, and G. Barruol (2008), SplitLab: A shear-wave splitting environment in Matlab, *Comput. Geosci.*, 34, 515–528.
- Zhang, S., and S.-i. Karato (1995), Lattice preferred orientation of olivine aggregates deformed in simple shear, *Nature*, 375(6534), 774–777.
- Zhu, H., and J. Tromp (2013), Mapping tectonic deformation in the crust and upper mantle beneath Europe and the North Atlantic ocean, *Science*, 341(6148), 871–875, doi:10.1126/science.1241335.
- Ziegler, P. A., and P. Dèzes (2006), Crustal evolution of Western and central Europe, *Geol. Soc. London Mem.*, 32(1), 43–56, doi:10.1144/GSL.MEM.2006.032.01.03.

Author Query Form

Journal: Journal of Geophysical Research: Solid Earth

Article: jgrb_51778

Dear Author,

During the copyediting of your paper, the following queries arose. Please respond to these by annotating your proofs with the necessary changes/additions.

- If you intend to annotate your proof electronically, please refer to the E-annotation guidelines.
- If you intend to annotate your proof by means of hard-copy mark-up, please refer to the proof mark-up symbols guidelines. If manually writing corrections on your proof and returning it by fax, do not write too close to the edge of the paper. Please remember that illegible mark-ups may delay publication.

Whether you opt for hard-copy or electronic annotation of your proofs, we recommend that you provide additional clarification of answers to queries by entering your answers on the query sheet, in addition to the text mark-up.

Query No.	Query	Remark
Q1	AUTHOR: Please complete the Publication Fee Consent Form included with your article and return to the Production Editor with your proofs.	
Q2	AUTHOR: Please confirm that given names (red) and surnames/family names (green) have been identified correctly.	
Q3	AUTHOR: Please check and confirm if the affiliations are presented appropriately.	